

---

# Papers

---

**Attenuation of  
wave-induced  
groundwater pressure  
in shallow water.  
Part 2. Theory**

OCEANOLOGIA, 47 (3), 2005.  
pp. 291–323.

© 2005, by Institute of  
Oceanology PAS.

**KEYWORDS**

Surface wave  
Pore water pressure  
Sandy beach  
Filtration  
Mathematical modelling

STANISŁAW R. MASSEL  
ANNA PRZYBORSKA  
MICHAŁ PRZYBORSKI

Institute of Oceanology,  
Polish Academy of Sciences,  
Powstańców Warszawy 55, PL-81-712 Sopot, Poland;  
e-mail: smas@iopan.gda.pl

Received 11 March 2005, revised 14 July 2005, accepted 17 August 2005.

## **Abstract**

In this Part 2 of the paper (Part 1 was published by Massel et al. 2004) an exact close-form solution for the pore-water pressure component and velocity circulation pattern induced by surface waves is developed. This comprehensive theoretical model, based on Biot's theory, takes into account soil deformations, volume change and pore-water flow. The calculations indicate that for the stiffness ratio  $\frac{G}{E'_w} \geq 100$ , the vertical distribution of the pore pressure becomes very close to the Moshagen & Tørum (1975) approach, when the soil is rigid and the fluid is incompressible.

The theoretical results of the paper have been compared with the experimental data collected during the laboratory experiment in the Large Wave Channel in Hannover (see Massel et al. 2004) and showed very good agreement. The apparent bulk modulus of pore water was not determined in the experiment but was estimated from the best fit of the experimental pore-water pressure with the theoretical one. In the paper only a horizontal bottom is considered and the case of an undulating bottom will be dealt with in another paper.

The complete text of the paper is available at <http://www.iopan.gda.pl/oceanologia/>

## 1. Introduction

Permeable sands are most common in the coastal environment and relict sands cover approximately 70% of the continental shelves. In particular, large volumes of sea water, driven by wave energy, are filtered by sandy beaches, and during this process the microfauna of the porous sand body mineralize organic materials in the water and recycle nutrients. High nutrient concentrations boost phytoplankton growth to generate about 30% of the total oceanic primary production in a zone covering less than 10% of the World Ocean (Huettel & Rusch 2000). Although the biodiversity and biomass of organisms within the beach body are low, it has been shown that marine sands transfer energy very effectively (Węśławski et al. 2000).

The velocity of flow as well as the amount of water circulating within the permeable beach body is important for the biological status of the organisms inhabiting the beach sand. Wave-induced pressure and stresses in seabeds are also important with regard to beach protection, design of foundations for gravity-type breakwaters and offshore oil storage tanks. They are the key elements when one considers the problem of flotation of buried pipelines and the burial of rubble mounds, tetrapods and other blocks by waves.

This paper presents a theoretical model of pore pressure attenuation within a sandy bottom and wave-induced groundwater circulation, initiated in Part 1 of the paper (Massel et al. 2004). There it was shown experimentally that there are two types of pore pressure induced by surface waves. At a water depth greater than the wave breaking depth, an instantaneous reaction of pore pressure (the so-called phase-resolving component) to wave motion is observed. To model this pressure component, Moshagen & Tørum (1975) described pressure attenuation in porous media, assuming the water to be compressible and the grain skeleton to be rigid. Using the special linearization technique for the Forchheimer equation for motion in porous media, Massel (1976) developed closed expressions for the geometry of the free surface, velocity components and pressure at any point in the flow, under the assumption of the potential theory. Recently, Li & Barry (2000) presented a numerical study of the instantaneous, phase-resolved wave motion and resulting groundwater flow in a beach zone as a result of a progressive bore.

In the surf zone, where waves break, the mean on-shore pressure gradient due to wave set-up drives a groundwater circulation within the beach body. This effect, though small, produces effects cumulative in time in the form of a slowly increasing pressure from an initial zero value to some asymptotic value (Longuet-Higgins 1983, Massel 2001, Massel et al. 2004). This pressure component is called the phase-averaged pressure, which depends on the gradient of the excess static pressure induced at the sea bottom due

to the wave set-up in the surf zone. However, this part of the pore pressure is not considered in the present paper.

The objective of the present study is to examine theoretically and experimentally the basic features of the instantaneous pore pressure (the phase-resolving component) and the wave-induced groundwater flow. This approach is based on Biot's linearized theory (Biot 1941, 1956), which takes into account soil deformations, volume change and pore-water flow. Some modifications of this theory have been discussed by Yamamoto et al. (1978), Madsen (1978), and Mei & Foda (1980, 1981).

To provide some reference for a physical understanding of the mechanism of groundwater circulation induced by wave motion, the model based on the assumptions that the soil skeleton obeys the laws of linear elasticity and the fluid obeys Darcy's law is used. This means that the case of low permeability is studied. The case of high permeability, when Darcy's law cannot be applied, should be treated by different methods.

The paper is organized as follows. Section 2 discusses the governing equations for groundwater pressure and its circulation. In particular, the attenuation of the phase-resolving pressure component and the water circulation pattern for constant water depth with a horizontal bottom and limited thickness of porous media is discussed. Section 3 compares the theoretical results with the experimental data obtained during laboratory measurements in the Large Wave Channel (GWK) in Hannover (Germany) and described in detail in Part 1 of this paper (Massel et al. 2004). Section 4 develops the coupled type model in which the boundary conditions at the sea bottom are described more precisely. Finally, Section 5 gives the summary and main conclusions.

## 2. Governing equations for wave-induced pressure and groundwater circulation

### 2.1. Biot's equations of linear poro-elasticity

In this Section we summarize briefly the wave-induced flow and stresses in a porous elastic medium using Biot's theory. So let us assume that the sand is isotropic and the flow is two-dimensional in the plane  $(0, x, z)$ . The origin of the Cartesian coordinates  $(x, z)$  is fixed on the mean free surface ( $z = 0$ ) and  $z$  is positive upwards – see Fig. 1. The water depth is  $h$  and the depth of the nonpermeable bottom is  $h_n$ . Thus, the thickness of the permeable layer is  $(h_n - h)$ . We assume that the coefficient of permeability and the porosity of sand are  $K_f$  and  $n$ , respectively.

We are interested in the small strains in soils, and particular soil grains are assumed to be incompressible, i.e. density of soil  $\rho_s = \text{constant}$ .

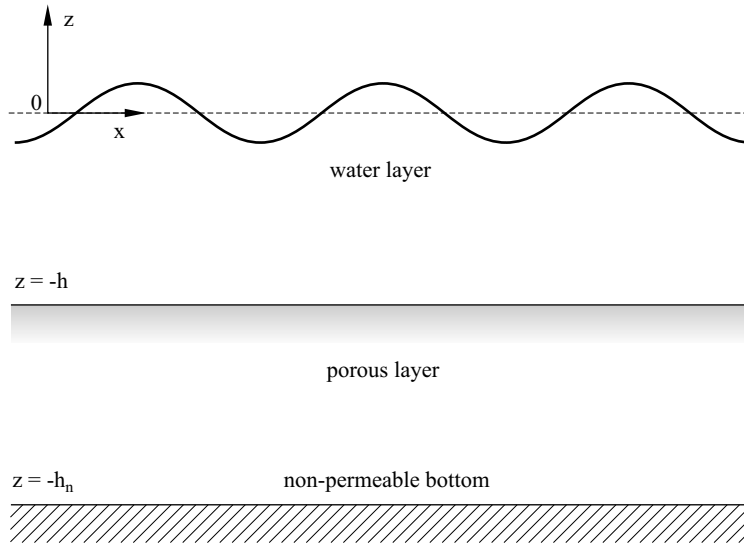


**Fig. 1.** Definition scheme

However, the soil matrix can still be compressible. In shallow water, due to possible wave breaking and the entrance of gases into the porous media and the production of gases by the organisms living in the sand, the apparent bulk modulus of the pore water  $E'_w$  depends on the degree of saturation by water  $S$ . In the relationship proposed by Verruijt (1969) we write:

$$\frac{1}{E'_w} = \frac{S}{E_w} + \frac{1 - S}{p_0}, \tag{1}$$

where  $E_w$  is the true bulk modulus of pore water without air and is equal to  $1.9 \times 10^9 \text{ N m}^{-2}$ ,  $(1 - S)$  is the degree of saturation by air, usually less than one, and  $p_0$  is the absolute pressure. For example, when  $S = 95\%$  (5% air content) and  $p_0 = 10^5 \text{ N m}^{-2}$ , the apparent bulk modulus of water is only  $E'_w = 2 \times 10^6 \text{ N m}^{-2}$ .

Many theoretical and experimental results indicate that the influence of the bottom permeability on sea surface elevation is rather small. This influence increases when the point under consideration approaches the permeable sea bottom, where the following boundary conditions should be satisfied:

$$\left. \begin{aligned} p_1(x, -h) &= p_2(x, -h) \\ \frac{\partial \Phi_1}{\partial z} &= nu_z \end{aligned} \right\}, \tag{2}$$

in which  $p_1$  and  $p_2$  are the dynamic pressures in the water column and porous media, respectively,  $\Phi_1$  is the velocity potential of wave motion in the water body,  $u_z$  is the vertical component of the pore water velocity and

$n$  is the sand porosity. Since the governing equations are valid only for materials finer than gravel, the vertical velocity  $u_z$  is very small and the second condition is taken to be  $\frac{\partial \Phi_1}{\partial z} = 0$ . So the motion in the water column and the porous media are connected only by the continuity of the dynamic pressure. This type of model is known as an uncoupled model. The coupled model, when both boundary conditions (2) are taken into account, will be discussed in Section 4.

Assuming now that  $E'_w$  is constant, we can represent the mass conservation equation in the form of the so-called storage equation (Mei & Foda 1981):

$$n \frac{\partial}{\partial x} (u_x - v_x) + \frac{\partial v_x}{\partial x} = -\frac{n}{E'_w} \frac{\partial p}{\partial t}, \quad (3)$$

$$n \frac{\partial}{\partial z} (u_z - v_z) + \frac{\partial v_z}{\partial z} = -\frac{n}{E'_w} \frac{\partial p}{\partial t}, \quad (4)$$

in which the sand porosity  $n$  is assumed to be constant,  $(u_x, u_z)$  are components of the velocity of the fluid,  $(v_x, v_z)$  are the components of the velocity of the soil matrix, and  $p$  is the pore pressure.

We adopt the linearized dynamic equations of momentum for fluid and soil in the following form (Mei & Foda 1981, Massel & Manzenrieder 1983, Massel 1985):

soil:

$$(1-n)\rho_s \frac{\partial v_x}{\partial t} = \frac{\partial \sigma_{xz}}{\partial z} - (1-n) \frac{\partial p}{\partial x} + \frac{n^2 \gamma}{K_f} (u_x - v_x), \quad (5)$$

$$(1-n)\rho_s \frac{\partial v_z}{\partial t} = \frac{\partial \sigma_{zx}}{\partial x} - (1-n) \frac{\partial p}{\partial z} + \frac{n^2 \gamma}{K_f} (u_z - v_z); \quad (6)$$

fluid:

$$n\rho_w \frac{\partial u_x}{\partial t} = -n \frac{\partial p}{\partial x} - \frac{n^2 \gamma}{K_f} (u_x - v_x), \quad (7)$$

$$n\rho_w \frac{\partial u_z}{\partial t} = -n \frac{\partial p}{\partial z} - \frac{n^2 \gamma}{K_f} (u_z - v_z), \quad (8)$$

where  $\sigma_{xz}$  and  $\sigma_{zx}$  are the effective stresses in the soil,  $\rho_s$  and  $\rho_w$  are the densities of soil and water, respectively,  $\gamma = \rho_w g$ , and  $K_f$  is the coefficient of filtration [ $\text{m s}^{-1}$ ]. It should be noted that the frictional resistance between soil and fluid is proportional to the local relative velocity, which is in agreement with Darcy's law. Thus, the model obeys the cases when laminar flow predominates.

Adopting Hooke's law for the effective stress and strain of the soil we obtain (Yamamoto 1977)

$$\sigma_x = 2G \left[ \frac{\partial \xi}{\partial x} + \frac{\nu}{1 - 2\nu} \epsilon \right], \quad (9)$$

$$\sigma_z = 2G \left[ \frac{\partial \eta}{\partial z} + \frac{\nu}{1 - 2\nu} \epsilon \right], \quad (10)$$

$$\tau_{xz} = G \left[ \frac{\partial \xi}{\partial z} + \frac{\partial \eta}{\partial x} \right], \quad (11)$$

in which  $\nu$  is the Poisson ratio,  $\xi$  and  $\eta$  are the  $x$  and  $z$  components of the soil displacement, respectively,  $\sigma_x$  is the effective normal stress in the  $x$ -direction,  $\sigma_z$  is the effective normal stress in the  $z$ -direction, and  $\tau_{xz}$  is the shearing stress in the  $z$ -direction on the plane with the normal in the  $x$ -direction, and  $\epsilon$  is the volume strain for the two-dimensional problem, i.e.

$$\epsilon = \frac{\partial \xi}{\partial x} + \frac{\partial \eta}{\partial z}. \quad (12)$$

The shear modulus of the soil  $G$  takes the form

$$G = \frac{E_s}{2(1 + \nu)}, \quad (13)$$

in which  $E_s$  is the Young's modulus of the soil.

From the effective stress concept and Hooke's law we obtain the following equations of equilibrium

$$G \nabla^2 \xi + \frac{G}{1 - 2\nu} \frac{\partial \epsilon}{\partial x} = \frac{\partial p}{\partial x}, \quad (14)$$

$$G \nabla^2 \eta + \frac{G}{1 - 2\nu} \frac{\partial \epsilon}{\partial z} = \frac{\partial p}{\partial z}, \quad (15)$$

where the pore water pressure satisfies the continuity equation

$$\nabla^2 p = \frac{\gamma}{K_f} \left[ \frac{n}{E'_w} \frac{\partial p}{\partial t} + \frac{\partial \epsilon}{\partial t} \right]. \quad (16)$$

Eqs. (14), (15) and (16) form a system of three partial differential equations for three unknowns:  $p$ ,  $\xi$  and  $\eta$ . To solve them we need to formulate appropriate boundary conditions. Since all the equations are linear, we employ complex variables in the analysis. However, it is implicitly assumed that only the real part of any complex quantity constitutes a solution to our problem. The linearity of the governing equations for propagating surface waves suggests that all variables will depend on  $x$  and  $t$  in the form  $\exp[i(kx - \omega t)]$ .

## 2.2. Boundary conditions

At the sea bottom line ( $z = -h$ ), the boundary conditions should express the physical fact that the effective vertical stress is zero, the shear stress is negligible and that wave-induced pressure fluctuations exists. Therefore at  $z = -h$  we have:

$$\sigma_z = 2G \left[ \frac{\partial \eta}{\partial z} + \frac{\nu}{1-2\nu} \left( \frac{\partial \xi}{\partial x} + \frac{\partial \eta}{\partial z} \right) \right] = 0, \quad (17)$$

$$\tau_{xz} = G \left[ \frac{\partial \xi}{\partial z} + \frac{\partial \eta}{\partial x} \right] = 0, \quad (18)$$

$$p = P_0 \exp [i(kx - \omega t)], \quad (19)$$

where  $P_0$  is the pressure amplitude at the bottom line,  $k$  is the wave number satisfying the dispersion relation

$$\omega^2 = gk \tanh(kh), \quad (20)$$

in which  $\omega$  is the surface wave frequency.

For simplicity the linear wave theory is used and the dynamic pressure in the water column ( $-h \leq z \leq 0$ ) takes the form

$$p(x, z, t) = \gamma \frac{H \cosh k(z+h)}{2 \cosh(kh)} \exp[i(kx - \omega t)], \quad (21)$$

in which  $H$  is the surface wave height. Therefore, at the sea bottom ( $z = -h$ ) we have

$$p(x, -h, t) = \gamma \frac{H}{2 \cosh(kh)} \exp[i(kx - \omega t)]; \quad (22)$$

thus

$$P_0 = \gamma \frac{H}{2 \cosh(kh)}. \quad (23)$$

We assume that the bed rock at  $z = -h_n$  is impermeable and rigid. Thus, soil displacements at this boundary are zero and no flow across the boundary is allowed, i.e.

$$\xi = \eta = 0, \quad (24)$$

$$\frac{\partial p}{\partial z} = 0. \quad (25)$$

## 2.3. Harmonic solution

To solve the boundary value problem for a system of three partial differential equations (14), (15) and (16) satisfying boundary conditions (17), (18), (19), (24) and (25), we use Yamamoto's (1977) approach. However, for the purpose of the present paper this approach has been modified substantially and misprints in his paper have been corrected. For

the boundary condition (19), periodic both in time and space, we assume that the soil displacements  $\xi$ ,  $\eta$  and pore pressure  $p$  are also periodic in time and space, i.e.

$$\xi(x, z, t) = \Re \{X(z) \exp[i(kx - \omega t)]\}, \quad (26)$$

$$\eta(x, z, t) = \Re \{Z(z) \exp[i(kx - \omega t)]\}, \quad (27)$$

$$p(x, z, t) = \Re \{P(z) \exp[i(kx - \omega t)]\}, \quad (28)$$

in which  $\Re$  denotes the real part of the complex quantity.

After substituting representations (26)–(28) in the governing equations (14)–(16) we obtain three simultaneous ordinary differential equations of the second order

$$G \frac{d^2 X}{dz^2} - \frac{2(1-\nu)G}{1-2\nu} k^2 X + i \frac{kG}{1-2\nu} \frac{dZ}{dz} - ikP = 0, \quad (29)$$

$$i \frac{Gk}{1-2\nu} \frac{dX}{dz} + \frac{2(1-\nu)G}{1-2\nu} \frac{d^2 Z}{dz^2} - Gk^2 Z - \frac{dP}{dz} = 0, \quad (30)$$

$$-k\omega X + i\omega \frac{dZ}{dz} + \frac{K_f}{\gamma} \frac{d^2 P}{dz^2} - \left[ \frac{K_f k^2}{\gamma} - i \frac{n\omega}{E'_w} \right] P = 0. \quad (31)$$

As the characteristic equation corresponding to the system (29)–(31) has repeated roots, we assume the general solution in the form

$$\begin{aligned} X(z) = & a_1 h \frac{\cosh k(z+h_n)}{\cosh kh_n} - a_2 h \frac{\sinh k(z+h_n)}{\sinh kh_n} \\ & - a_3(z+h) \frac{\cosh k(z+h_n)}{\cosh kh_n} + a_4(z+h) \frac{\sinh k(z+h_n)}{\sinh kh_n} \\ & + a_5 h \frac{\cosh \psi(z+h_n)}{\cosh \psi h_n} - a_6 h \frac{\sinh \psi(z+h_n)}{\sinh \psi h_n}, \end{aligned} \quad (32)$$

$$\begin{aligned} Z(z) = & b_1 h \frac{\cosh k(z+h_n)}{\cosh kh_n} - b_2 h \frac{\sinh k(z+h_n)}{\sinh kh_n} \\ & - b_3(z+h) \frac{\cosh k(z+h_n)}{\cosh kh_n} + b_4(z+h) \frac{\sinh k(z+h_n)}{\sinh kh_n} \\ & + b_5 h \frac{\cosh \psi(z+h_n)}{\cosh \psi h_n} - b_6 h \frac{\sinh \psi(z+h_n)}{\sinh \psi h_n}, \end{aligned} \quad (33)$$

$$\begin{aligned} P(z) = & c_1 P_0 \frac{\cosh k(z+h_n)}{\cosh kh_n} - c_2 P_0 \frac{\sinh k(z+h_n)}{\sinh kh_n} \\ & - c_3 P_0 \frac{z+h}{h} \frac{\cosh k(z+h_n)}{\cosh kh_n} + c_4 P_0 \frac{z+h}{h} \frac{\sinh k(z+h_n)}{\sinh kh_n} \\ & + c_5 P_0 \frac{\cosh \psi(z+h_n)}{\cosh \psi h_n} - c_6 P_0 \frac{\sinh \psi(z+h_n)}{\sinh \psi h_n}, \end{aligned} \quad (34)$$

in which

$$\psi^2 = k^2 \left\{ 1 - i \frac{\omega\gamma}{k^2 K_f} \left[ \frac{n}{E'_w} + \frac{1}{G} \frac{1-2\nu}{2(1-\nu)} \right] \right\}. \quad (35)$$

It should be noted that the coefficients  $a_n$ ,  $b_n$ ,  $c_n$  ( $n = 1 \dots 6$ ) are not independent. Their dependence was determined by the substitution of eqs. (32), (33) and (34) in eqs. (29)–(31), from which the following relationships were obtained

$$\left. \begin{aligned} b_1 &= i \left[ \coth(kh_n) a_2 - \frac{A_1}{h} a_3 \right] & b_2 &= i \left[ \tanh(kh_n) a_1 - \frac{A_1}{h} a_4 \right] \\ b_3 &= i \coth(kh_n) a_4 & b_4 &= i \tanh(kh_n) a_3 \\ b_5 &= i \left( \frac{\psi}{k} \right) \coth(\psi h_n) a_6 & b_6 &= i \left( \frac{\psi}{k} \right) \tanh(\psi h_n) a_5 \end{aligned} \right\} \quad (36)$$

and

$$\left. \begin{aligned} c_1 &= -i \frac{A_2 \coth(kh_n)}{P_0} a_4 & c_2 &= -i \frac{A_2 \tanh(kh_n)}{P_0} a_3 \\ c_3 &= 0 & c_4 &= 0 \\ c_5 &= -\frac{A_3 h}{P_0} a_5 & c_6 &= -\frac{A_3 h}{P} a_6 \end{aligned} \right\}, \quad (37)$$

where

$$A_1 = \frac{1}{k} \frac{1 + \frac{3-4\nu}{1-2\nu} \frac{nG}{E'_w}}{1 + \frac{1}{1-2\nu} \frac{nG}{E'_w}}, \quad (38)$$

$$A_2 = \frac{2G}{1 + \frac{1}{1-2\nu} \frac{nG}{E'_w}}, \quad (39)$$

$$A_3 = \frac{2(1-\nu)}{1-2\nu} \frac{\omega G}{kc}, \quad (40)$$

in which

$$c = \frac{K_f}{\gamma} \left[ \frac{n}{E'_w} + \frac{1-2\nu}{2(1-\nu)G} \right]^{-1}. \quad (41)$$

Now we have to determine the six constants  $a_n$  ( $n = 1 \dots 6$ ) from the boundary conditions (17)–(19) and (24)–(25). Thus we obtain:

at the sea bottom ( $z = -h$ ):

$$\frac{1-\nu}{1-2\nu} \frac{dZ}{dz} + \frac{\nu}{1-2\nu} ikX = 0, \quad (42)$$

$$\frac{dX}{dz} + ikZ = 0, \quad (43)$$

$$P = P_0; \quad (44)$$

at a non-porous bottom ( $z = -h_n$ ):

$$\left. \begin{array}{l} X = 0 \\ Z = 0 \\ \frac{dP}{dz} = 0 \end{array} \right\}. \quad (45)$$

After substituting eqs. (32)–(34) in the boundary conditions (42)–(45) and using the relationships (36)–(37), we obtain the following system of six simultaneous equations for coefficients  $a_j$ :

$$d_{ij} a_j = e_i; \quad i = 1, 6, \quad j = 1, 6, \quad (46)$$

where

$$e_i = \begin{cases} P_0 & \text{for } i = 1, \\ 0 & \text{for } i > 1. \end{cases} \quad (47)$$

The matrix coefficients  $d_{ij}$  are given in Appendix (A).

The solution of the system of equations (46) provides the coefficients  $a_j$  and subsequently, the amplitudes of the excess pore water pressure  $P(z)$  and soil displacements  $X(z)$  and  $Z(z)$ .

## 2.4. Specific cases

### 2.4.1. Soil completely saturated with water

As follows from the definitions of coefficients  $A_1$ ,  $A_2$  and  $A_3$ , the leading quantity controlling the behaviour of solutions (32)–(34) is the stiffness ratio,  $\frac{G}{E'_w}$ . When the soil is completely saturated with water and the pore-water does not contain gases, the stiffness  $\frac{G}{E'_w} \rightarrow 0$ . In this case, the apparent modulus of elasticity  $E'_w$  is equal to the true modulus of elasticity of water,  $E_w = 1.9 \times 10^9 \text{ N m}^{-2}$  and the value of  $G$  for soils varies from about  $10^8 \text{ N m}^{-2}$  for very dense sand to  $10^5 \text{ N m}^{-2}$  for silt and clay.

To examine the governing equation for pore-pressure, let us introduce the following non-dimensional variables:

$$\tilde{x} = \frac{x}{L}, \quad \tilde{z} = \frac{z}{L}, \quad \tilde{t} = \omega t \quad (48)$$

and

$$\tilde{p} = \frac{p}{P_0}, \quad \begin{bmatrix} \tilde{v}_x \\ \tilde{v}_z \end{bmatrix} = \frac{G}{P_0 \omega L} \begin{bmatrix} v_x \\ v_z \end{bmatrix}, \quad (49)$$

in which  $L$  is the length of the surface wave.

After substituting in the non-dimensional variables (16) we obtain

$$\nabla^2 \tilde{p} - \frac{\gamma n \omega L^2}{K_f E'_w} \frac{\partial \tilde{p}}{\partial \tilde{t}} - \frac{\gamma \omega L^2}{K_f G} \left( \frac{\partial \tilde{v}_x}{\partial \tilde{x}} + \frac{\partial \tilde{v}_z}{\partial \tilde{z}} \right) = 0 \quad (50)$$

or

$$\nabla^2 \tilde{p} - \frac{\gamma \omega L^2}{K_f G} \left[ \frac{nG}{E'_w} \frac{\partial \tilde{p}}{\partial \tilde{t}} + \left( \frac{\partial \tilde{v}_x}{\partial \tilde{x}} + \frac{\partial \tilde{v}_z}{\partial \tilde{z}} \right) \right] = 0. \quad (51)$$

For  $\frac{G}{E'_w} \rightarrow 0$ , eq. (51) simplifies as follows:

$$\nabla^2 \tilde{p} - \frac{\gamma \omega L^2}{K_f G} \left( \frac{\partial \tilde{v}_x}{\partial \tilde{x}} + \frac{\partial \tilde{v}_z}{\partial \tilde{z}} \right) = 0. \quad (52)$$

It should be noted that for fully saturated gravel and coarse sand, when  $K_f$  is rather high, eq. (52) is further simplified to the Laplace equation

$$\nabla^2 \tilde{p} = 0 \quad \text{and} \quad \nabla^2 p = 0. \quad (53)$$

Hence, the pore-water pressure response for completely saturated coarse soils ( $\frac{G}{E'_w} \rightarrow 0$ ) is the same as that obtained by Putman (1949), who assumed that soil is rigid and water is incompressible. The pressure attenuation for this case is very small and independent of the soil permeability. However, when  $K_f$  is very small, as is the case for fully saturated fine sand, the pressure attenuation is associated with the soil deformation (see eq. (52)).

To find the solution of eq. (53), we use the expressions (37)–(40) for  $\frac{G}{E'_w} \rightarrow 0$ . Hence we get  $A_1 = k^{-1}$ ,  $A_2 = 2G$ ,  $A_3 = 0$ , and

$$\begin{aligned} c_1 &= -i \frac{2G}{P_0} \coth(kh_n) a_4, & c_2 &= -i \frac{2G}{P_0} \tanh(kh) a_3; \\ c_3 &= c_4 = c_5 = c_6 = 0. \end{aligned} \quad (54)$$

From the last equation of the system (46) we obtain  $a_3 = 0$ , thus  $c_2 = 0$ .

On the other hand, the first equation of this system gives  $a_4 = i \frac{P_0 \sinh(kh_n)}{A_2 \cosh k(h_n - h)}$  and  $c_1 = \frac{\cosh kh_n}{\cosh k(h_n - h)}$ . Hence, for the pore pressure from eq. (34) we get

$$P(z) = P_0 \frac{\cosh k(z + h_n)}{\cosh k(h_n - h)}. \quad (55)$$

When the porous layer becomes a semi-infinite half-plane, i.e.  $h_n \rightarrow \infty$ , eq. (55) yields

$$P(z) = P_0 \exp[k(z + h)]. \quad (56)$$

#### 2.4.2. Soil saturated with a mixture of liquid and gas

In the other extreme case, when dense sand is saturated with a mixture of liquid and gas, the stiffness of the soil becomes much larger than that of the pore fluid, i.e.  $\frac{G}{E'_w} \rightarrow \infty$ . As follows from eq. (1), for sand 95%

saturated with water at atmospheric pressure, the apparent modulus of elasticity equals  $E'_w \sim 2 \times 10^6 \text{ N m}^{-2}$ . Therefore, for dense sand, when  $G \sim 10^8 \text{ N m}^{-2}$ , the stiffness ratio  $\frac{G}{E'_w} \approx 100$ .

The governing equation for pore pressure for this extreme case can be obtained from eq. (50) which we rewrite in a slightly different form:

$$\nabla^2 \tilde{p} - \frac{\gamma n \omega L^2}{K_f E'_w} \left[ \frac{\partial \tilde{p}}{\partial \tilde{t}} + \frac{E'_w}{nG} \left( \frac{\partial \tilde{v}_x}{\partial \tilde{x}} + \frac{\partial \tilde{v}_z}{\partial \tilde{z}} \right) \right] = 0. \quad (57)$$

Thus, for  $\frac{G}{E'_w} \rightarrow \infty$  we get

$$\nabla^2 \tilde{p} - \frac{\gamma n \omega L^2}{K_f E'_w} \frac{\partial \tilde{p}}{\partial \tilde{t}} = 0 \quad (58)$$

or in dimensional form

$$\nabla^2 p - \frac{n \gamma}{K_f E'_w} \frac{\partial p}{\partial t} = 0. \quad (59)$$

Using representation (28), eq. (59) becomes

$$\frac{d^2 P(z)}{dz^2} - k^2 \left( 1 - i \frac{n \gamma \omega}{k^2 K_f E'_w} \right) P(z) = 0. \quad (60)$$

When  $\frac{G}{E'_w} \rightarrow \infty$ , from eqs. (38)–(40) we obtain

$$A_1 = \frac{3 - 4\nu}{k}, \quad A_2 = 0, \quad A_3 \rightarrow \infty. \quad (61)$$

The last equation of the set (46) and relationships (37) give  $a_6 = 0$  and  $c_6 = 0$ . On the other hand, from the fifth equation of the set (46) we have  $a_5 = -\frac{P_0}{h} \frac{\cosh(\psi h_n)}{\cosh \psi(h_n - h)}$  and  $c_5 = P_0 \frac{\cosh \psi(z + h_n)}{\cosh \psi(h_n - h)}$ . After substituting the above relationships in eq. (34) and using the fact that  $c_1 = c_2 = c_3 = c_4 = 0$ , we obtain

$$P(z) = P_0 \frac{\cosh \psi(z + h_n)}{\cosh \psi(h_n - h)}. \quad (62)$$

For  $\frac{G}{E'_w} \rightarrow \infty$ , the wave number  $\psi$  defined by eq. (35) becomes

$$\psi^2 \approx \psi_1^2 = k^2 \left[ 1 - i \frac{n \gamma \omega}{k^2 K_f E'_w} \right] \quad (63)$$

and

$$P(z) = P_0 \frac{\cosh \psi_1(z + h_n)}{\cosh \psi_1(h_n - h)}, \quad (64)$$

which for  $h_n \rightarrow \infty$ , becomes

$$P(z) = P_0 \exp[\psi_1(z + h)]. \quad (65)$$

Depending on the stiffness ratio,  $\frac{G}{E'_w}$ , the soil permeability and the gas content in the pore water, the transmission of pressure stresses and deformation in the sediment falls somewhere in between the above two extreme cases.

## 2.5. Velocities of groundwater circulation and water particle displacements

### 2.5.1. Groundwater velocity components

Gradients of pore-water pressure induce a pore-water circulation in porous media. The flow velocities can be derived from eqs. (7) and (8). First of all, using the definitions of the soil displacements  $\xi$  and  $\eta$ , we have

$$v_x = \frac{\partial \xi}{\partial t} = -i\omega X(z) \exp[i(kx - \omega t)], \quad (66)$$

$$v_z = \frac{\partial \eta}{\partial t} = -i\omega Z(z) \exp[i(kx - \omega t)]. \quad (67)$$

As the boundary condition (19) is periodic both in time and space, we assume the pore water velocity to take the form

$$\left. \begin{aligned} u_x(x, z, t) &= \Re \{U_x(z) \exp[i(kx - \omega t)]\}, \\ u_z(x, z, t) &= \Re \{U_z(z) \exp[i(kx - \omega t)]\}. \end{aligned} \right\} \quad (68)$$

After substituting eqs. (66)–(68) in eqs. (7)–(8) we obtain

$$U_x(z) = \frac{kP(z)K_f + n\omega\gamma X(z)}{\rho_w\omega K_f + in\gamma}, \quad (69)$$

$$U_z(z) = \frac{n\omega\gamma Z(z) - i \frac{dP(z)}{dz} K_f}{\rho_w\omega K_f + in\gamma}. \quad (70)$$

The term  $\rho_w\omega K_f$  in the denominator of eqs. (69) and (70) is usually much smaller than  $n\gamma$ ; therefore,  $\rho_w\omega K_f + in\gamma \approx in\gamma$ .

Now, the above equations can be rewritten as follows:

$$U_x(z) = |U_x(z)| \exp[i(\varphi_{U_x} - \pi/2)], \quad (71)$$

$$U_z(z) = |U_z(z)| \exp[i(\varphi_{U_z} + \pi)], \quad (72)$$

where

$$|U_x(z)| = \left| \frac{kP(z)}{n\gamma} + \frac{\omega X(z)}{K_f} \right| K_f, \quad (73)$$

$$|U_z(z)| = \left| \frac{dP(z)}{dz} + i \frac{\omega Z(z)}{K_f} \right| K_f \quad (74)$$

and

$$\varphi_{U_x}(z) = \arg(U_x(z)) \text{ and } \varphi_{U_z}(z) = \arg(U_z(z)).$$

Therefore, from eqs. (68) we obtain

$$u_x(x, z, t) = |U_x(z)| \sin(kx - \omega t + \varphi_{U_x}) \quad (75)$$

and

$$u_z(x, z, t) = -|U_z(z)| \cos(kx - \omega t + \varphi_{U_z}). \tag{76}$$

The absolute total pore water velocity becomes

$$u(x, z, t) = \sqrt{u_x^2(x, z, t) + u_z^2(x, z, t)}. \tag{77}$$

Assuming that we can ignore the soil displacements i.e.  $X(z) = Z(z) = 0$ , from eqs. (73) and (74), we get

$$|U_x(z)| \approx \left| \frac{kP(z)}{n\gamma} \right| K_f = \frac{k}{n\gamma} |P(z)| K_f \tag{78}$$

and

$$|U_z(z)| \approx \left| \frac{dP(z)}{dz} \right| K_f = \frac{1}{n\gamma} \left| \frac{dP(z)}{dz} \right| K_f. \tag{79}$$

Moreover, for phase lags  $\varphi_{U_x}(z)$  and  $\varphi_{U_z}(z)$ , we obtain

$$\varphi_{U_x}(z) = \arg(P(z)) \quad \text{and} \quad \varphi_{U_z}(z) = \arg\left(\frac{dP(z)}{dz}\right). \tag{80}$$

### 2.5.2. Pore water particle velocity versus soil skeleton velocity

For surface waves of sufficiently high frequency almost all the fluid in the interior of the soil is strongly resisted by viscosity and usually cannot have a significant velocity, when comparing to the soil skeleton velocity. Therefore, the difference between the pore fluid and the soil becomes negligibly small. However, in the layer close to the sea bottom, drainage is much easier and relative motion can be appreciable within this thin layer.

In order to examine the attenuation of pore water velocity components  $u_x$  and  $u_z$ , and the soil velocities  $v_x$  and  $v_z$ , let us write the differences of the corresponding components in the form

$$\Delta u_x = u_x - v_x = \Re \left\{ \frac{kP(z)}{in\gamma} K_f \exp[i(kx - \omega t)] \right\} \tag{81}$$

or

$$\Delta u_x = \frac{k|P(z)|}{n\gamma} K_f \exp \left[ i \left( kx - \omega t + \varphi_{U_x}(z) - \frac{\pi}{2} \right) \right] \tag{82}$$

and

$$\Delta u_z = u_z - v_z = \Re \left\{ -\frac{dP(z)}{dz} \frac{K_f}{n\gamma} \exp [i(kx - \omega t)] \right\} \tag{83}$$

or

$$\Delta u_z = \left| \frac{dP(z)}{dz} \right| \frac{K_f}{n\gamma} \exp [i(kx - \omega t + \varphi_{U_z}(z) + \pi)]. \tag{84}$$

The vertical attenuation of the differences between pore water velocity and soil skeleton velocity  $\Delta u_x$  and  $\Delta u_z$  is driven by the attenuation of the pore water pressure  $P(z)$  and its gradient  $\frac{dP(z)}{dz}$ . Mei & Foda (1980, 1981) used the differences  $\Delta u_x$  and  $\Delta u_z$  to develop a boundary layer theory in the porous media similar to the approach well known in the dynamics of viscous fluids. They showed that the poro-elastic problem may be reduced first by solving a conventional elastostatic problem, when  $\Delta u_x = \Delta u_z$  (fluid and solid move together), and then making a boundary layer correction near the sea bottom when  $\Delta u_x \neq 0$  and  $\Delta u_z \neq 0$ .

### 2.5.3. Displacements of pore water particles

Consider now the pore water particle, whose position is denoted by  $(x_0, z_0)$ . The particle orbits are determined by assuming that the motion around a fixed point  $(x_0, z_0)$  is small, so that one can consider  $x$  and  $z$  constant in the integration. Hence, we have

$$x = \int_0^t u_x dt \quad \text{and} \quad z = \int_0^t u_z dt. \quad (85)$$

Substituting (75) and (76) in (85) we obtain

$$x = x_0 + \frac{1}{\omega} |U_x| \cos(kx - \omega t + \varphi_{U_x}), \quad (86)$$

$$z = z_0 + \frac{1}{\omega} |U_z| \sin(kx - \omega t + \varphi_{U_z}). \quad (87)$$

Eqs. (86) and (87) can be rewritten in the form

$$\frac{(x - x_0)^2}{A^2} + \frac{(z - z_0)^2}{B^2} + 2 \frac{(x - x_0)(z - z_0)}{C^2} \sin(\Delta\varphi) = 1.0, \quad (88)$$

in which

$$A = \left(\frac{1}{\omega}\right) |U_x| \cos(\Delta\varphi), \quad (89)$$

$$B = \left(\frac{1}{\omega}\right) |U_z| \cos(\Delta\varphi), \quad (90)$$

$$C = \left(\frac{1}{\omega}\right) \sqrt{|U_x||U_z|} \cos(\Delta\varphi), \quad \text{and} \quad (91)$$

$$\Delta\varphi = \varphi_{U_x} - \varphi_{U_z}. \quad (92)$$

In fact eq. (88) represents an elliptical contour with its centre at point  $(x_0, z_0)$ . In order to confirm that, let us present this equation in traditional form

$$\frac{(x - x_0)^2}{A_1^2} + \frac{(z - z_0)^2}{B_1^2} = 1.0, \quad (93)$$

where the semi-axes become

$$A_1 = 2 \left(\frac{1}{\omega}\right) \frac{|U_x||U_z| \cos(\Delta\varphi)}{\sqrt{U_a}}, \quad (94)$$

$$B_1 = 2 \left( \frac{1}{\omega} \right) \frac{|U_x| |U_z| \cos(\Delta\varphi)}{\sqrt{U_b}}, \tag{95}$$

$$U_a = 2(|U_x|^2 + |U_z|^2) - \sqrt{4(|U_x|^4 + |U_z|^4) - 2(3 + \cos(2\Delta\varphi))|U_x|^2 |U_z|^2}, \tag{96}$$

$$U_b = 2(|U_x|^2 + |U_z|^2) + \sqrt{4(|U_x|^4 + |U_z|^4) - 2(3 + \cos(2\Delta\varphi))|U_x|^2 |U_z|^2}. \tag{97}$$

The quantities  $A_1$  and  $B_1$  represent the large and small semi-axes of the ellipse contour, respectively. When  $\frac{G}{E_w} \rightarrow 0$ , the phase lags  $\varphi_{U_x}$  and  $\varphi_{U_z}$  are both equal to zero. Therefore, from eqs. (96) and (97) we get

$$\left. \begin{aligned} A_1 &= \left( \frac{1}{\omega} \right) |U_x| \\ \text{and} \\ B_1 &= \left( \frac{1}{\omega} \right) |U_z| \end{aligned} \right\}. \tag{98}$$

Eq. (93), with  $A_1$  and  $B_1$  given by (98), represents the closed elliptical contour with axes parallel to the corresponding coordinate axes.

### 3. Comparison with experimental data

During a controlled large-scale laboratory experiment carried out in Large Wave Channel in Hannover (see Part 1 of this paper for details), an extensive data set was collected. For comparison with the theoretical model developed in this paper, a total of 23 tests were selected. They are related to the pressure gauge system 4 located on the beach at water depth  $h = 2$  m. The incident wave height and wave period vary as  $0.2 \text{ m} < H_{in} < 0.8 \text{ m}$  and  $5.0 \text{ s} < T < 10.0 \text{ s}$ . To obtain the water pressure at the sea bottom the incident wave height was transferred to the water depth  $h = 2$  m at the pressure gauge system position using the linear wave theory.

As follows from the sand sample characteristics given in Part 1 of this paper, the beach body was formed from fine-grained, well sorted sand of porosity  $n = 0.26$  and Young’s modulus  $E_s \approx 10^8 \text{ N m}^{-2}$ . The coefficient  $K_f$  was estimated in the laboratory test using sand from the channel. This procedure gives the value of the intrinsic permeability  $K \approx 3.1 \times 10^{-11} \text{ m}^2$  (K. Czerniak, personal communication). To obtain the filtration coefficient  $K_f$ , a known relationship between  $K$  and  $K_f$  was used

$$K_f = K \frac{g}{\nu_1}, \tag{99}$$

in which  $\nu_1$  is the kinematic coefficient of viscosity. For sea water of salinity  $S = 35$  ppm and of temperature  $T = 20^\circ\text{C}$ , the coefficient

$\nu_1 = 1.064 \times 10^{-6} \text{ m}^2 \text{ s}^{-1}$  (Massel 1999); therefore, the coefficient of filtration  $K_f$  becomes  $K_f = 2.9 \times 10^{-4} \text{ m s}^{-1}$ .

This value corresponds closely to the filtration coefficient  $K_f$  resulting from the well-known Hazen formula (Massel 2001)

$$K_f \approx 0.5 D_{10}^2, \quad (100)$$

in which  $K_f$  is in metres per second and the characteristic diameter  $D_{10}$  is in centimetres. Using  $D_{10} = 2.1 \times 10^{-2} \text{ cm}$  (Massel et al. 2004), we obtain  $K_f \approx 2.2 \times 10^{-4} \text{ m s}^{-1}$ , which is very close to the value obtained in the laboratory test.

The degree of saturation of air in the pore water was not measured directly in the experiments, but the apparent bulk modulus of water  $E'_w$  was estimated from the best fit of the experimental pore pressures to the theoretical ones. The comparison made for all 23 tests showed that  $4 \times 10^5 \text{ N m}^{-2} \leq E'_w \leq 1.6 \times 10^6 \text{ N m}^{-2}$ .

Using these values in eq. (1) yields a very high degree of saturation by air. However, there is serious doubt about the applicability of eq. (1) to the sandy beach artificially formed in the wave channel. In fact the sand used in the experiment cannot be regarded as natural sand as was assumed in Verruijt's (1969) formula. It is very probable that during sand layering in the wave channel, some pores within the beach body will be saturated by air/gas microbubbles.

From extensive field measurements of wave-induced pore pressure for water depths of approximately 5–10 m and to a depth of approximately 18 m below the sea bottom carried out by de Rouck & Troch (2002), it follows that there was approximately 3% gas in the soil pores. However, in laboratory conditions, the air/gas content can be in the range 3–10% (Tørum, submitted).

As follows from eq. (1), for an isotropic sand layer, the  $E'_w$  value should be approximately constant as the variation in ambient pressure  $p$  with submergence in the beach sand is insignificant. In order to check this fact, we determined the  $E'_w$  values which yield a minimal difference between the theoretical and experimental values of the pore pressure for particular pressure gauge levels. For illustration, the resulting values of  $E'_w$  for Tests 2 and 10 are given in Table 1.

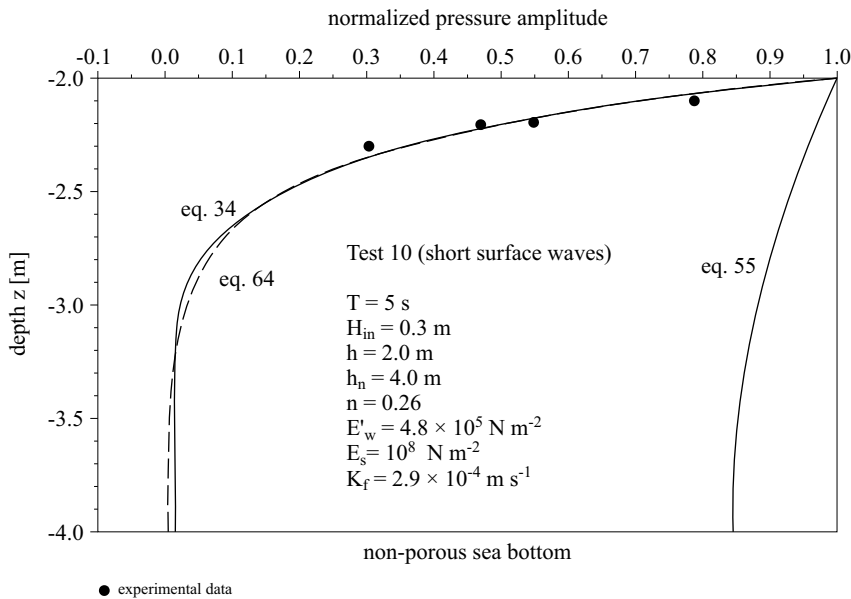
The  $E'_w$  values are different for particular levels and attenuate with gauge submergence in the porous layer. This result suggests that the apparent bulk modulus  $E'_w$  of pore water depends not only on the air content, as follows from eq. (1), but also on other factors which are unknown at present.

During the Hannover experiment, the stiffness ratio  $\frac{G}{E'_w}$  varied between 50 and 400. It was shown that for  $\frac{G}{E'_w} \geq 50$ , the vertical distribution of the pore pressure was very close to the distribution given by eq. (64), identical

**Table 1.** The apparent bulk modulus of pore water  $E'_w$  at different submergence of pressure gauges

Submergence of pressure gauges [m]	Test 2 ( $H_{in} = 0.5$ m, $T = 8$ s)		Test 10 ( $H_{in} = 0.3$ m, $T = 5$ s)	
	$E'_w(z)$	mean value	$E'_w(z)$	mean value
$z_1 = -2.1$	$5.9 \times 10^5$	$2.8 \times 10^5$	$9.8 \times 10^5$	$4.8 \times 10^5$
$z_2 = -2.205$	$2.4 \times 10^5$		$4.2 \times 10^5$	
$z_3 = -2.195$	$3.2 \times 10^5$		$6.0 \times 10^5$	
$z_4 = -2.3$	$2.2 \times 10^5$		$3.6 \times 10^5$	

to the solution obtained by Moshagen & Tørum (1975) when the soil is rigid and the fluid is compressible. This is illustrated in Figs 2 and 3. In Fig. 2 the vertical distribution of the amplitude of the pore-water pressure for both special cases resulting from eqs. (55) and (64) are shown for short waves (Test 10: period  $T = 5$  s, incident wave height  $H_{in} = 0.3$  m). The attenuation of pore-water pressure for the case of fully saturated soils (eq. (55)) is small and independent of the soil permeability. When the soil is partly saturated with a mixture of water and gas (eq. (64)), pore pressure attenuates very rapidly. In the same figure, the full solution (34) for Test

**Fig. 2.** Comparison between experiment and theory with respect to pore pressure for Test 10 (short surface waves)

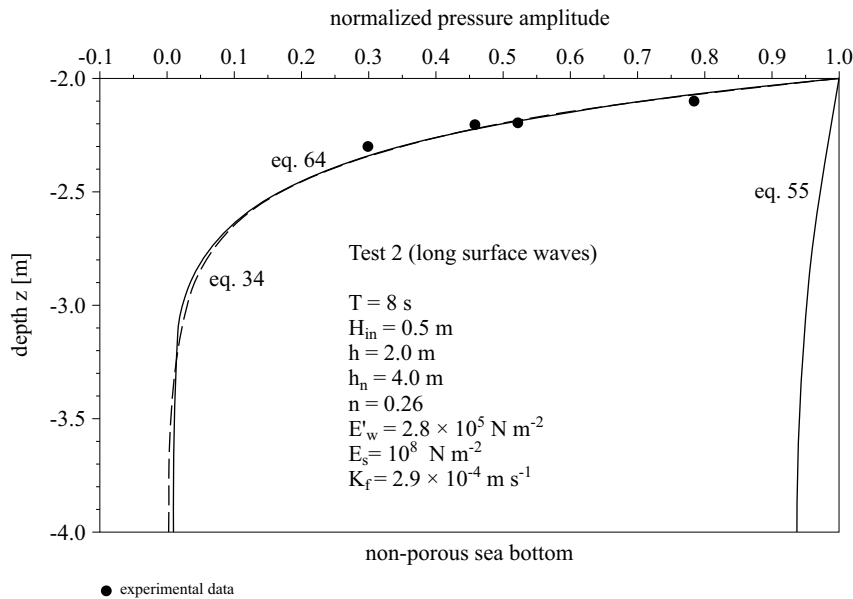


**Fig. 3.** Comparison between experimental and theory with respect to pore pressure for Test 2 (long surface waves)

10 with the stiffness ratio  $\frac{G}{E'_w} \approx 78$  is shown. Solution (34) is very close to the solution for a partly saturated soil when  $\frac{G}{E'_w} \rightarrow \infty$  and compares very well with the experimental data.

The results for the case of longer waves (Test 2: period  $T = 8$  s and incident wave height  $H_{in} = 0.5$  m) is demonstrated in Fig. 3. Now the stiffness ratio  $\frac{G}{E'_w} \approx 134$  and the pore pressures resulting from solutions (34) and (64) are almost identical.

Figs 4a, 4b and 4c compare the theoretical and experimental absolute values of pore pressure for different submergences of the pressure gauges for 24 tests. The theoretical values were calculated using the mean bulk modulus of the pore water  $E'_w$  resulting from the best fit of the experimental and theoretical pore pressures for all the gauges used in the experiment. In other words, the selected  $E'_w$  values correspond to the average degree of saturation by air in a porous layer extending from sea bottom to 0.3 m below the bottom. The figures illustrate the approximately linear dependence of the absolute pore pressure on the local wave height. At levels  $z_1 = -2.1$  m and  $z_2 = -2.195$  m, the experimental pore pressure is slightly higher than the theoretical one. The opposite tendency is observed at level  $z_3 = -2.3$  m. In all cases the difference between the theoretical and experimental values is smaller than  $200 \text{ N m}^{-2}$ . In the figures, the lines (solid and broken) present the best fit of the theoretical and experimental data, respectively.

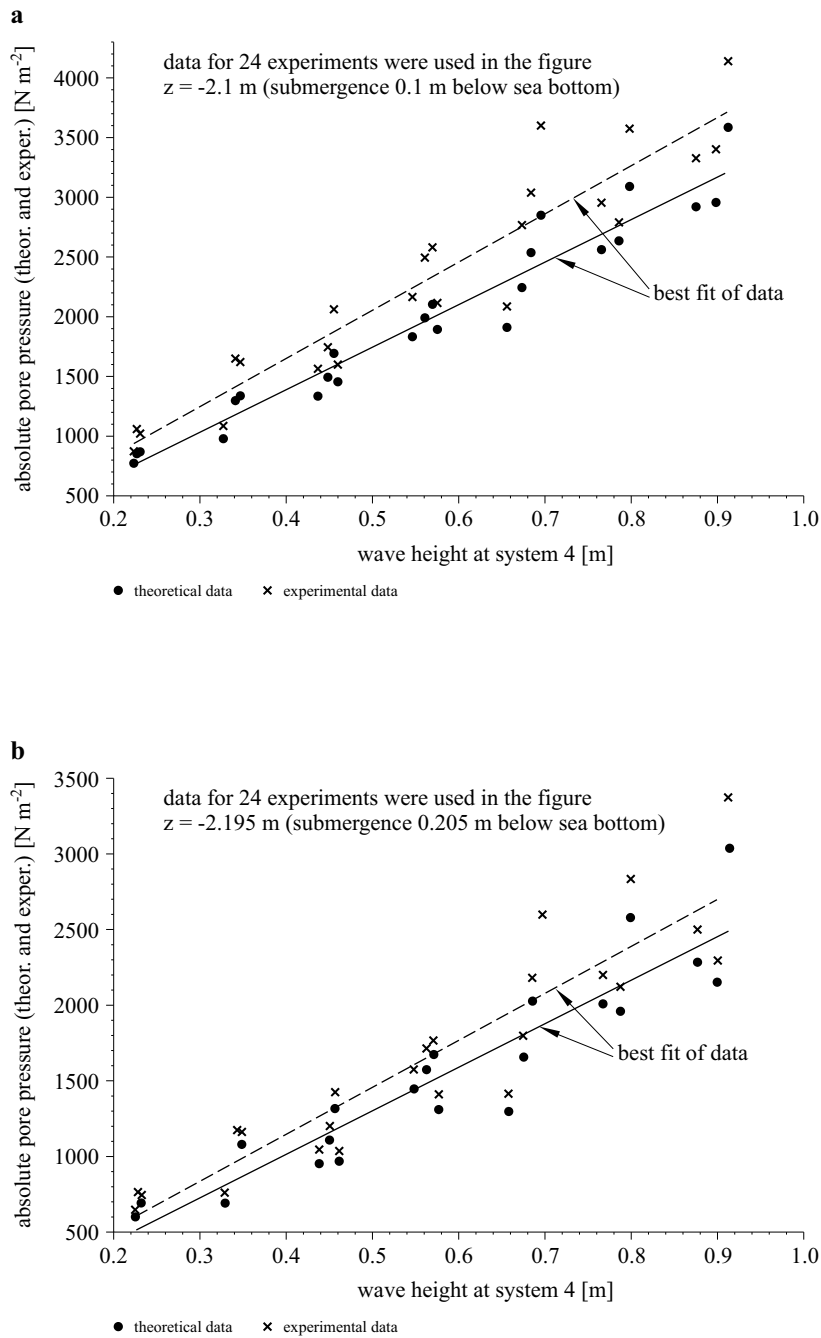


**Fig. 4.** Comparison of experimental and theoretical data with respect to pore pressure: (a) gauge at level  $z = -2.1$  m (submergence 0.1 m below sea bottom); (b) gauge at level  $z = -2.195$  m (submergence 0.195 m below sea bottom); (c) gauge at level  $z = -2.3$  m (submergence 0.3 m below sea bottom)

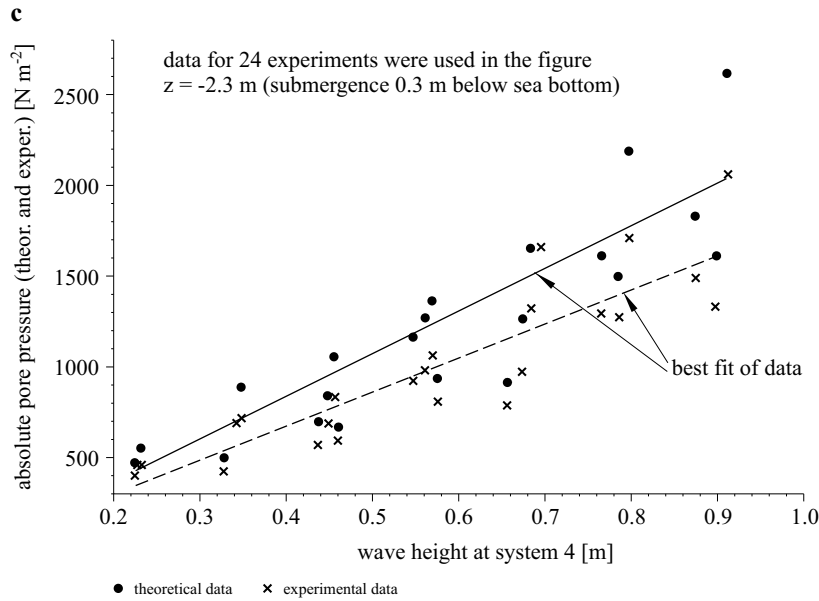


**Fig. 4.** (*continued*)

The slight scattering of the data around the best fit lines indicates that the pore water pressure depends not only on the incident wave height but also on the mechanical properties of the soil and liquid, which should be expected.

Fig. 5 presents the vertical distribution of the phase lag for pore pressure when measured against the wave crest (Test 2). For completely saturated soil the phase lag is equal to zero. However, for pore water containing air, the phase lag increases almost linearly with distance from the sea bottom, except in the vicinity of the non-porous bottom. Fig. 6 gives the absolute values of the corresponding vertical displacements of both components of soil displacements, i.e.  $\xi$  (in the  $x$ -direction) and  $\eta$  (in the  $z$ -direction).

Fig. 7 shows the normalized velocity components  $u_x(0, z, t)/K_f$  and  $u_z(0, z, t)/K_f$  resulting from eqs. (75)–(76) for Test 10 at level  $z = -2.1$  m (0.1 m below the sea bottom). The figure demonstrates that the horizontal velocity component is very small when compared with the vertical velocity component. Additionally, Fig. 8 gives the vertical distribution of the differences  $\Delta u_x$  and  $\Delta u_z$  between the pore water and soil skeleton velocities for Test 10. The difference between the horizontal velocity components  $u_x$  and  $v_x$  becomes negligibly small 1 m below the sea bottom, while the difference between the vertical velocity components are larger and only 1.5 m below the sea bottom does this difference become practically zero.

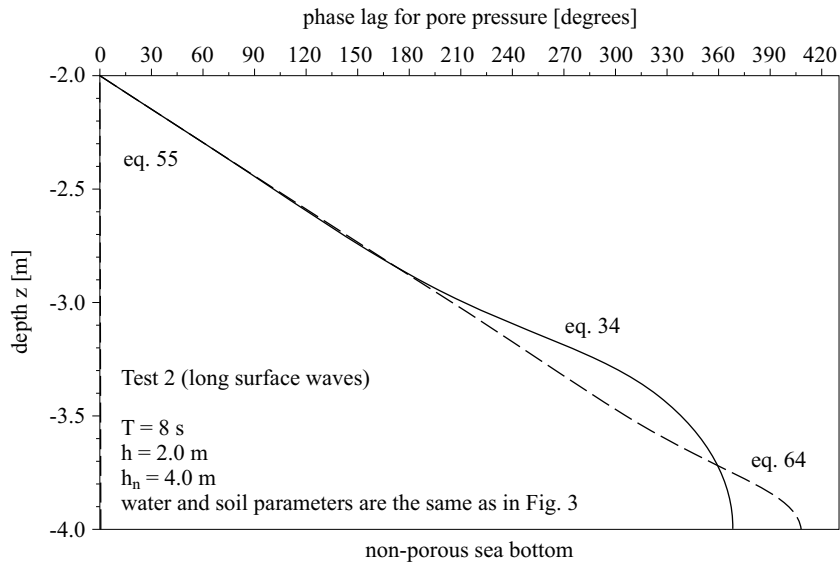


Fig. 5. Vertical distribution of phase lag for pore pressure

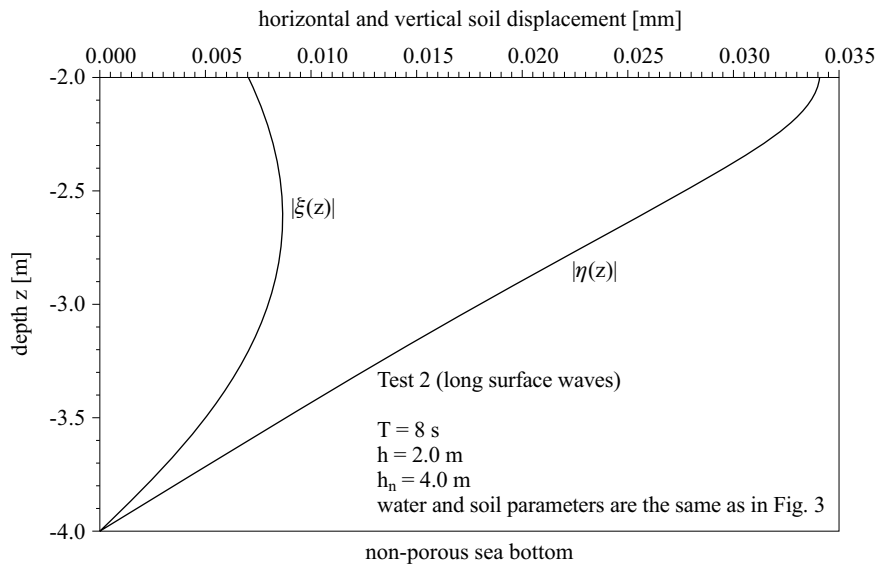
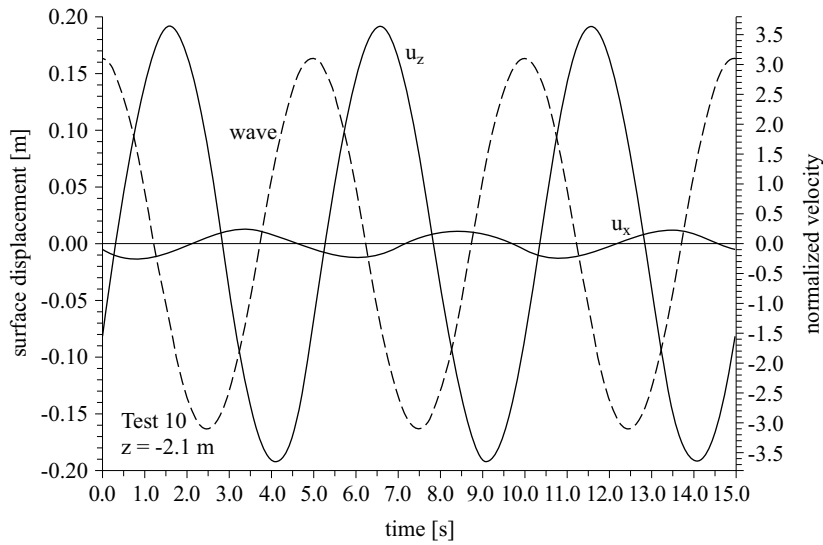
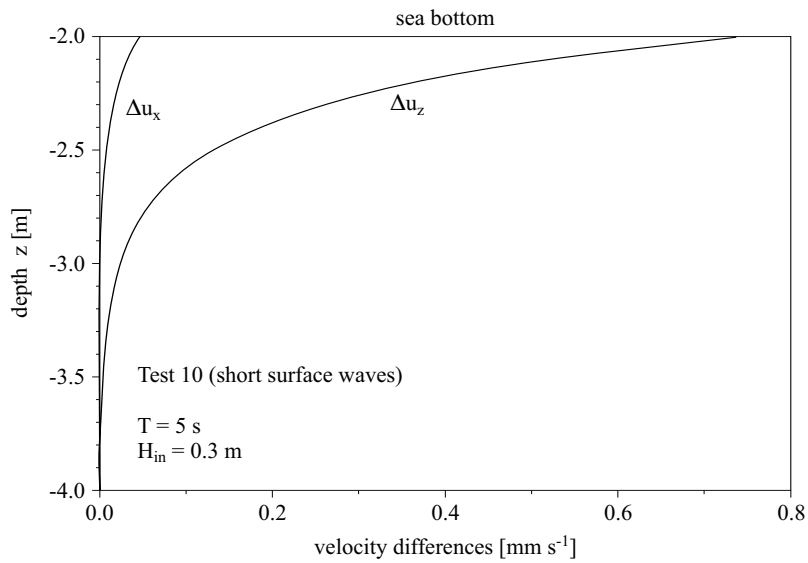


Fig. 6. Vertical and horizontal displacements of soil displacements for Test 2

As follows from eqs. (73)–(79), the pressure gradients  $\frac{dP}{dx}$  and  $\frac{dP}{dz}$  are the leading terms for determining the pore water velocities. The theoretical velocities with approximate velocities calculated using the experimental pore pressure gradients for the point located 0.2 m below the sea bottom



**Fig. 7.** Velocity components and total velocity for Test 10 (short surface waves)



**Fig. 8.** Vertical distribution of the differences between horizontal and vertical components of the pore water and soil skeleton velocities

( $z = -2.2$  m) are compared in Fig. 9. The approximate velocities are calculated as follows:

$$u_x(x, z, t) \approx \frac{1}{n\gamma} \frac{p(x + 0.1, z, t) - p(x - 0.1, z, t)}{2\Delta x} \quad (101)$$

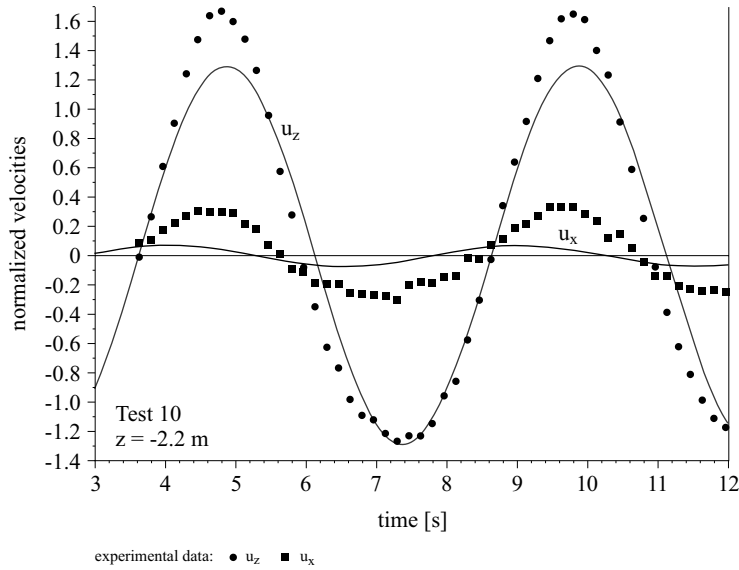


**Fig. 9.** Comparison of theoretical and approximate normalized velocities at level  $z = -2.2$  m for Test 10

and

$$u_z(x, z, t) \approx \frac{1}{n\gamma} \frac{p(x, z + 0.1, t) - p(x, z - 0.1, t)}{2\Delta z} \quad (102)$$

in which  $\Delta x = \Delta z = 0.1$  m,  $x = 0$ ,  $z = -2.2$  m.

As the wave motion and pore pressure were not recorded in the same profile, the zero value of the theoretical time series of the vertical velocity was fitted with the zero value of the approximate vertical velocity. From the figure it follows that the approximate vertical velocity agrees with the theoretical one except in the regions of positive maximum velocity. This is probably a demonstration of the nonlinear effects in the wave motion. In Test 10, the ratio  $\frac{L}{h} = 10$ , which corresponds to nonlinear Stokes waves rather than to the linear waves used in the model. The approximate values of the horizontal velocity components are higher than those resulting from the theory. This is a slightly surprising result as the two points used for calculating the horizontal gradient are only 0.2 m apart and are located at the same level  $z = -2.2$  m.

Finally, using relationships (86) and (87), the water particle orbits at 0.1 m below the sea bottom ( $z = -2.1$  m) are shown in Fig. 10. The water particles move along inclined closed elliptical contours owing to the assumption of periodic wave motion. The inclination of the elliptical contour reflects the phase lag between wave surface oscillation and pore pressure.

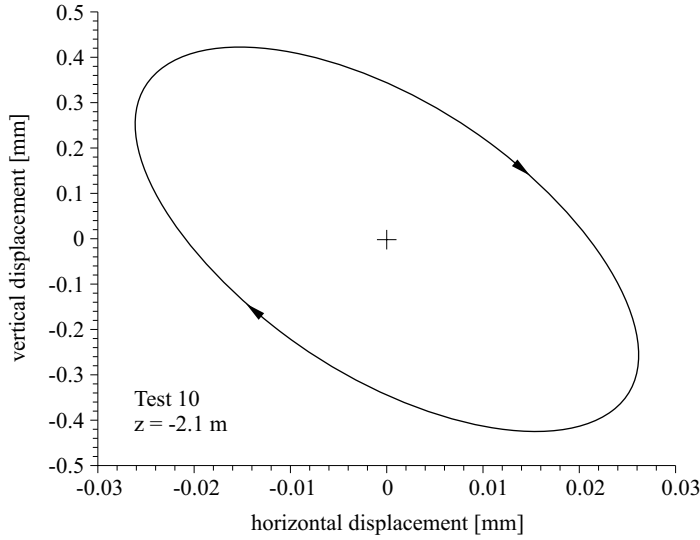


**Fig. 10.** Pore water particle circulation pattern for the sea bottom level (Test 10,  $z = -2.1$  m)

#### 4. Coupled model for pore pressure attenuation in the porous layer

##### 4.1. The boundary value problem and its solution

In the model developed in Section 2, the solutions in the water and porous layers are subject to boundary conditions (17)–(19) at  $z = -h$ . Therefore, the continuity is restricted to the pore pressure only, and the vertical and horizontal components of the water velocity become discontinuous. This kind of model is considered to be an uncoupled model. It would be interesting to check the extent to which the pore pressure and pore water circulation depend on the boundary conditions at  $z = -h$ . Therefore, let us formulate a model when the full boundary conditions (2) are satisfied. In particular, in the water layer we assume an irrotational flow represented by the Laplace equation for the potential function  $\Phi_1$ . Hence, we have

$$\frac{\partial^2 \Phi_1}{\partial x^2} + \frac{\partial^2 \Phi_1}{\partial z^2} = 0; \quad -\infty < x < \infty; \quad -h \leq z \leq 0 \quad (103)$$

with the linearized water surface conditions as follows:

$$\left. \begin{aligned} \frac{\partial^2 \Phi_1}{\partial t^2} + g \frac{\partial \Phi_1}{\partial z} &= 0 \\ \frac{\partial \Phi_1}{\partial t} + g \zeta_1 &= 0 \end{aligned} \right\} z = 0. \quad (104)$$

At the sea surface, a regular wave train is assumed, hence

$$\zeta_1 = \Re \frac{H}{2} \exp[i(kx - \omega t)]. \tag{105}$$

The boundary conditions (2) should be satisfied at the sea bottom.

Let us represent the velocity potential  $\Phi_1$  as follows (Massel 1976):

$$\Phi_1(x, z, t) = [A \cosh k(z + h) + B \sinh k(z + h)] \exp[i(kx - \omega t)]. \tag{106}$$

In the porous layer we assume that the stiffness ratio  $\frac{G}{E_w} \gg 1$ . Hence the pore pressure and pore water velocity components become (see eqs. (64) and (68))

$$p_2(x, z, t) = \Re P(z) \exp[i(kx - \omega t)], \tag{107}$$

$$u_x(x, z, t) = \Re \left\{ -i \frac{K_f k}{n\gamma} P(z) \exp[i(kx - \omega t)] \right\} \tag{108}$$

and

$$u_z(x, z, t) = \Re \left\{ -\frac{K_f}{n\gamma} \frac{dP(z)}{dz} \exp[i(kx - \omega t)] \right\}. \tag{109}$$

The continuity of the dynamic pressure and vertical velocity component at  $z = -h$  requires that

$$A = -i \frac{P_0}{\rho\omega} \quad \text{and} \quad B = -\frac{K_f}{\gamma} \left( \frac{\psi_1}{k} \right) \tanh[\psi_1(h_n - h)] P_0, \tag{110}$$

in which the wave number  $\psi_1$  is defined by eq. (63).

After substituting the above values in the second condition (104) we obtain

$$P_0 = \frac{i \frac{gH}{2\omega}}{\frac{i}{\rho\omega} \cosh(kh) + \frac{K_f}{\gamma} \left( \frac{\psi_1}{k} \right) \tanh[\psi_1(h_n - h)] \sinh(kh)} \tag{111}$$

or

$$P_0 = \frac{i\rho gH}{2 \left[ i \cosh(kh) + \frac{K_f \omega}{g} \left( \frac{\psi_1}{k} \right) \tanh[\psi_1(h_n - h)] \sinh(kh) \right]}. \tag{112}$$

If the porous media are non-porous ( $K_f = 0$ ), the above equations simplify considerably. Thus, we have:

$$\left. \begin{aligned} A &= -i \frac{P_0}{\rho\omega} = -i \frac{gH}{2\omega \cosh(kh)}; \quad B = 0 \\ \Phi_1 &= \frac{-igH}{2\omega} \frac{\cosh k(z + h)}{\cosh kh} \exp[i(kx - \omega t)] \\ \omega^2 &= gk \tanh(kh) \end{aligned} \right\}. \tag{113}$$

Eqs. (113) represent the classical boundary value problem for regular waves propagating in a water layer of constant depth  $h$  over a non-porous bottom.

## 4.2. Dispersion relation

The unknown complex wave number  $k$  is described by the dispersion relation, which can be obtained from the first condition (104). Hence, we have

$$\omega^2 = gk \frac{A \tanh(kh) + B}{A + B \tanh(kh)} \quad (114)$$

or

$$\omega^2 = gk \frac{\tanh(kh) + \frac{B}{A}}{1 + \frac{B}{A} \tanh(kh)} \quad (115)$$

in which

$$\frac{B}{A} = -i \frac{\omega K_f}{g} \left( \frac{\psi_1}{k} \right) \tanh[\psi_1(h_n - h)]. \quad (116)$$

The solution of the dispersion relation (115) is given by the complex wave number  $k = k_r + ik_i$ . For example, for Test 2 ( $H_{in} = 0.5$  m,  $T = 8$  s), the wave number becomes  $k = 0.181415 + 0.000298i$ , while when the uncoupled model is used, the wave number  $k = 0.181116$  (see eq. (20)). Also, the calculations for all tests carried out during the Hannover experiment showed that the real value of the wave number  $k_r$  is almost identical with the wave number  $k$  resulting from the uncoupled model, while the imaginary part of the wave number  $k_i$  is of the order of 0.0001–0.0003. Substituting these values in eq. (105) we obtain

$$\begin{aligned} \zeta_1 &= \frac{H}{2} \exp[i(k_r + ik_i)x] \exp(-\omega t) = \\ &= \frac{H}{2} \exp(-k_i x) \exp[i(k_r x - \omega t)]. \end{aligned} \quad (117)$$

From eq. (117) it follows that the wave amplitude attenuates by 1% over a distance of about 50 m for  $k_i = 0.0002 \text{ m}^{-1}$ .

The above estimate of the wave number  $k$  in the coupled model suggests that the permeability of the sea bottom does not substantially influence the length of the surface wave.

## 4.3. Pore water velocity components

In contrast to the wavelength, there is a difference in the velocities at the sea bottom predicted by both models. In the uncoupled model the vertical velocity  $u_z(x, -h, t) = 0$  when approaching the sea bottom in the water layer, while in the coupled model we have

$$u_z(x, -h, t) = \frac{\partial \Phi_1}{\partial z} = k B \exp[i(kx - \omega t)] \quad (118)$$

or

$$u_z(x, -h, t) = -\frac{\psi_1 K_f}{\gamma} \tanh[\psi_1(h_n - h)] P_0. \quad (119)$$

For the cases tested in the Hannover experiment, the vertical velocity is of the order of  $1 \text{ mm s}^{-1}$  (see, for example, Figs 7 and 8).

The horizontal velocity components in water and porous layers, predicted by the uncoupled model for  $z = -h$  (sea bottom), are also different; hence, we have

$$\begin{aligned} \Delta u_x = u_x^{(1)} - u_x^{(2)} = \frac{kP_0}{\rho\omega} \exp[i(kx - \omega t)] + \\ + i \frac{kP_0}{\gamma} K_f \exp[i(kx - \omega t)] \end{aligned} \quad (120)$$

or

$$\Delta u_x = \left( \frac{g}{\omega} + iK_f \right) \frac{kP_0}{\gamma} \exp[i(kx - \omega t)], \quad (121)$$

in which  $u_x^{(1)}$  and  $u_x^{(2)}$  are the horizontal velocity components in the water and porous layer, respectively.

The first term in the parentheses is simply the phase velocity of the surface waves in deep water and is much higher than the coefficient of permeability  $K_f$ . Thus, the velocity difference becomes approximately

$$\Delta u_x \approx \frac{gkP_0}{\omega\gamma} = \frac{1}{2} \frac{\omega H}{\sinh(kh)} \exp[i(kx - \omega t)]. \quad (122)$$

#### 4.4. Horizontal velocity component within the boundary layer at the sea bed

It should be noted that the horizontal component of velocity in the water layer follows from the assumption of the irrotational motion in this layer. However, in the close proximity of the porous bed, a viscous boundary layer of thickness  $\delta$  of the order ( $O\sqrt{\nu_1/\omega}$ ) forms;  $\nu_1$  is the kinematic coefficient of viscosity. The flow inside the boundary layer can be essentially considered as horizontal. If we neglect the non-linear, convective acceleration term, the equation of motion within the boundary layer can be written as follows (Kaczmarek 1999):

$$\frac{\partial u_x^{(b)}}{\partial t} - \nu \frac{\partial^2 u_x^{(b)}}{\partial z^2} = \frac{\partial u_{x,\infty}}{\partial t}, \quad (123)$$

in which  $u_x^{(b)}$  is the horizontal velocity within the boundary layer,  $u_{x,\infty}$  is the ambient flow at the upper limit of the boundary layer and  $\nu$  is the kinematic viscosity coefficient. Thus, at the boundary layer limit we have

$$u_{x,\infty} = \frac{1}{2} \frac{\omega H}{\sinh kh} \exp[i(kx - \omega t)]. \quad (124)$$

Let

$$u_x^{(b)}(x, z, t) = U_x^{(b)}(z) \exp[i(kx - \omega t)]. \quad (125)$$

After substituting eqs. (124) and (125) in (123) we obtain

$$\frac{d^2 U_x^{(b)}}{dz^2} + \psi_0^2 U_x^{(b)} = D_0, \quad (126)$$

in which

$$\psi_0^2 = i \frac{\omega}{\nu} \quad (127)$$

and

$$D_0 = i \frac{\omega^2 H}{2\nu \sinh(kh)}. \quad (128)$$

The solution of eq. (126) becomes

$$U_x^{(b)}(z) = C_1 \cos(\psi_0 z) + C_2 \sin(\psi_0 z) + \frac{D_0}{\psi_0^2} \{1 - \cos[\psi_0(z+h)]\}. \quad (129)$$

The constants  $C_1$  and  $C_2$  should be determined from the boundary conditions at  $z = -h$  (sea bottom) and  $z = -h + \delta$  (upper limit of the boundary layer), i.e.

$$U_x^{(b)} = \begin{cases} \frac{1}{2} \frac{\omega H}{\sinh(kh)} & \text{at } z = -h + \delta, \\ -i \frac{kH K_f}{2 \cosh(kh)} & \text{at } z = -h. \end{cases} \quad (130)$$

The calculations yield

$$C_1 = \frac{R_1 \sin(\psi_0 h) - R_2 \sin[\psi_0(h - \delta)]}{\sin(\psi_0 \delta)} \quad (131)$$

and

$$C_2 = \frac{R_1 \cos(\psi_0 h) - R_2 \cos[\psi_0(h - \delta)]}{\sin(\psi_0 \delta)}, \quad (132)$$

in which

$$R_1 = \frac{1}{2} \frac{\omega H}{\sinh(kh)} - \frac{D_0}{\psi_0^2} [1 - \cos(\psi_0 \delta)], \quad (133)$$

$$R_2 = \frac{-i}{2} \frac{kH K_f}{\cosh(kh)}. \quad (134)$$

It should be noted that the boundary layer thickness  $\delta$  is of the order of  $\sqrt{\frac{\nu}{\omega}}$ . Thus for the typical wave frequency, it can be obtained  $\delta \approx 1$  mm. Conditions (17) and (18) indicate that the boundary layer in the porous media was neglected when approaching the sea bottom ( $z \rightarrow -h$ ) for  $\frac{g}{E'_w} \gg 1$ . Therefore, in the calculations, the continuity of horizontal velocity is presented in the form of the second equation (130).

## 5. Summary and conclusion

In this paper an exact close-form solution has been obtained for the pore-water pressure and velocities induced by surface waves in the elastic porous layer. This solution is related to the so-called phase-resolving pore pressure component when the pore pressure responds instantaneously to the sea surface variation and the slowly varying pressure component is neglected. This means that the solution is valid for coastal waters outside the breaker zone. The analytical solution taking into account soil deformations, volume change and pore-water flow is based on Biot's theory.

Comparison of the theoretical results with laboratory measurements in the Large Wave Channel (GWK) in Hannover, described in Part 1 of the paper, shows very good agreement. In particular, the differences between the theoretical and experimental pore pressures are  $< \text{ca } 200 \text{ Pa}$ . The theoretical calculations for the experimental cases indicate that the horizontal component of the pore-water velocity is smaller than the vertical one. On the assumption of periodic wave motion, the water particles circulate along closed, inclined elliptical contours.

The stiffness ratio  $\frac{G}{E'_w}$  is the parameter controlling pore-water behaviour under surface wave loading. When  $\frac{G}{E'_w} \geq 100$ , the vertical distribution of the pore pressure becomes very close to the Moshagen & Tørum (1975) solution when the soil is rigid and the fluid is compressible. Almost all the cases treated during the GWK experiment resulted in a stiffness ratio of  $\frac{G}{E'_w} > 100$  when the simple heat transfer type equation (59) was applied.

The value of the apparent bulk modulus of pore water  $E'_w$  was not determined in the experiments but was estimated from the best fit of the experimental pore-water pressure with the theoretical one. The fit showed that the modulus  $E'_w$  is of the order of  $10^5$ – $10^6 \text{ N m}^{-2}$ . When this value is used in (1), a high air content of the order of 10% is obtained. This is probably due to the fact that eq. (1) is not applicable to the case of a beach body artificially formed in the wave channel, which is not the case with natural sand.

In this paper, only the case of a horizontal bottom was studied. The case of the non-horizontal bottom will be dealt with in a separate paper.

## Acknowledgements

The large-scale tests at the LARGE WAVE CHANNEL (GWK) of the Coastal Research Centre (FZK) were supported by the European Community under the Access to Research Infrastructures Action of the Human Potential Programme (contract HPRI-CT-2001-00157). The theoretical analysis in the paper is a part of the Coastal Sands as Biocatalytical

Filters project (COSA) supported by the European Community through the contract EKV3-CT-2002-00076 and by the Ministry of Science and Information Technology of Poland under the contract SPB/5.PR UE/DIE 43. The Authors express their sincere gratitude for the financial support.

## References

- Biot M. A., 1941, *General theory of three-dimensional consolidation*, J. Appl. Phys., 12, 155–164.
- Biot M. A., 1956, *Theory of propagation of elastic waves in a fluid-saturated porous solid. Part 1: Low frequency range. Part 2: Higher frequency range*, J. Acoust. Soc. Am., 28 (2), 168–191.
- De Rouck J., Troch P., 2002, *Pore water pressure response due to tides and waves based on prototype measurements*, PIANC Bull., 110, 9–31.
- Huettel M., Rusch A., 2000, *Transport and degradation of phytoplankton in permeable sediment*, Limnol. Oceanogr., 45 (3), 534–549.
- Kaczmarek L. M., 1999, *Moveable sea bed boundary layer and mechanics of sediment transport*, Wyd. Inst. Bud. Wod. PAN, Gdańsk, 209 pp.
- Li L., Barry D. A., 2000, *Wave-induced beach groundwater flow*, Adv. Water Res., 23, 325–337.
- Longuet-Higgins M. S., 1983, *Wave set-up, percolation and undertow in the surf zone*, Proc. R. Soc., Lond., A390, 283–291.
- Madsen O. S., 1978, *Wave induced pore pressures and effective stresses in a porous bed*, Geotechnique, 28 (4), 377–393.
- Massel S. R., 1976, *Gravity waves propagated over a permeable bottom*, J. Waterway Div.–ASCE, 102, 111–121.
- Massel S. R., 1985, *Soil boundary layer – applications in ocean engineering*, Arch. Hydrotech., 32 (2), 157–194, (in Polish).
- Massel S. R., 2001, *Circulation of groundwater due to wave set-up on a permeable beach*, Oceanologia, 43 (3), 279–290.
- Massel S. R., Manzenrieder M., 1983, *Scattering of surface waves by a submerged cylindrical body with porous screen*, Rep. No 562, Leichtweiss Inst. Wasserbau, Gdańsk–Braunschweig, 56 pp.
- Massel S. R., Przyborska A., Przyborski M., 2004, *Attenuation of wave-induced groundwater pressure in shallow water. Part 1*, Oceanologia, 46 (3), 383–404.
- Mei C. C., Foda M. A., 1980, *Boundary layer theory of waves in a poro-elastic sea bed*, Proc. Int. Symp. ‘Soils under Cyclic and Transient Loading’, 7–11 January, Swansea, 609–618.
- Mei C. C., Foda M. A., 1981, *Wave-induced responses in a fluid-filled poro-elastic solid with a free surface – a boundary layer theory*, Geophys. J. Roy. Astron. Soc., 66, 597–631.
- Moshagen H., Tørum A., 1975, *Wave-induced pressures in permeable seabeds*, J. Waterway Div.–ASCE, 101, 49–57.

- Putman J. A., 1949, *Loss of wave energy due to percolation in a permeable sea bottom*, Trans. Am. Geophys. Union, 30, 349–356.
- Tørum A., *Wave induced pore pressure – air/gas content*, J. Waterw. Port Coast. Ocean Eng., (submitted).
- Verruijt A., 1969, *Elastic storage of aquifers*, [in:] *Flow through porous media*, R. J. M. Dewiest (ed.), Acad. Press, New York, 331–376.
- Węśławski J. M., Urban-Malinga B., Kotwicki L., Opaliński K., Szymelfening M., Dutkowski M., 2000, *Sandy coastlines – are there conflicts between recreation and natural values?*, Oceanol. Stud., 29(2), 5–18.
- Yamamoto T., 1977, *Wave-induced instability in sea beds*, Proc. Spec. Conf. ‘Coastal Sediments’, 898–913.
- Yamamoto T., Koning H. L., Sellmeier H., Hijum E. V., 1978, *On the response of a poro-elastic bed to water waves*, J. Fluid Mech., 87, 193–206.

**Appendix (A)**

The matrix  $d_{ij}$  coefficients for the system of simultaneous equations (46):

$$d_{11} = 0; \quad d_{21} = 2kh \frac{\sinh k(h_n - h)}{\cosh kh_n} \quad (\text{A.1})$$

$$d_{31} = ikh(1 - 2\nu) \frac{\cosh k(h_n - h)}{\cosh kh_n}; \quad d_{41} = \frac{h}{\cosh kh_n} \quad (\text{A.2})$$

$$d_{51} = 0; \quad d_{61} = 0 \quad (\text{A.3})$$

$$d_{12} = 0; \quad d_{22} = -2kh \frac{\cosh k(h_n - h)}{\sinh kh_n} \quad (\text{A.4})$$

$$d_{32} = ikh(2\nu - 1) \frac{\sinh k(h_n - h)}{\sinh kh_n}; \quad d_{42} = 0 \quad (\text{A.5})$$

$$d_{52} = i \frac{h}{\sinh kh_n}; \quad d_{62} = 0 \quad (\text{A.6})$$

$$d_{13} = i \frac{A_2 \sinh k(h_n - h)}{\cosh kh_n}; \quad d_{23} = (kA_1 - 1) \frac{\cosh k(h_n - h)}{\cosh kh_n} \quad (\text{A.7})$$

$$d_{33} = i(kA_1 - 1)(1 - \nu) \frac{\sinh k(h_n - h)}{\cosh kh_n}; \quad d_{43} = \frac{(h_n - h)}{\cosh kh_n} \quad (\text{A.8})$$

$$d_{53} = -i \frac{A_1}{\cosh kh_n}; \quad d_{63} = i \frac{kA_2}{\cosh kh_n} \quad (\text{A.9})$$

$$d_{14} = -i \frac{A_2 \cosh k(h_n - h)}{\sinh kh_n}; \quad d_{24} = \frac{(1 - kA_1) \sinh k(h_n - h)}{\sinh kh_n} \quad (\text{A.10})$$

$$d_{34} = i \frac{(kA_1 - 1)(\nu - 1) \cosh k(h_n - h)}{\sinh kh_n}; \quad d_{44} = 0 \quad (\text{A.11})$$

$$d_{54} = i \frac{h_n - h}{\sinh kh_n}; \quad d_{64} = 0 \quad (\text{A.12})$$

$$d_{15} = -\frac{A_3 h \cosh \psi(h_n - h)}{\cosh \psi h_n}; \quad d_{25} = 2h\psi \frac{\sinh \psi(h_n - h)}{\cosh \psi h_n} \quad (\text{A.13})$$

$$d_{35} = -i \frac{h[\nu k^2 + (\nu - 1)\psi^2] \cosh \psi(h_n - h)}{k \cosh \psi h_n}; \quad d_{45} = \frac{h}{\cosh \psi h_n} \quad (\text{A.14})$$

$$d_{55} = 0; \quad d_{65} = 0 \quad (\text{A.15})$$

$$d_{16} = \frac{A_3 h \sinh \psi(h_n - h)}{\sinh \psi h_n}; \quad d_{26} = -\frac{2h\psi \cosh \psi(h_n - h)}{\sinh \psi h_n} \quad (\text{A.16})$$

$$d_{36} = i \frac{h[\nu k^2 + (\nu - 1)\psi^2] \sinh \psi(h_n - h)}{k \sinh \psi h_n}; \quad d_{46} = 0 \quad (\text{A.17})$$

$$d_{56} = \frac{ih\psi}{k \sinh \psi h_n}; \quad d_{66} = \frac{A_3 h \psi}{\sinh \psi h_n}. \quad (\text{A.18})$$